Proceedings of the Sixteenth International Conference on
Computational Structures Technology
Edited by: P. Iványi, J. Kruis and B.H.V. Topping
Civil-Comp Conferences, Volume 14, Paper 11.1
Civil-Comp Press, Edinburgh, United Kingdom, 2026
ISSN: 2753-3239, doi: 10.4203/ccc.14.11.1

Programmable Multifunctional Hyperbolic Metamaterials: Design and Optimization

M. Yang, L. Meng, X. Zhu, W. Zhu, Z. Cai, J. Zhu and W. Zhang

State IJR Center of Aerospace Design and Additive Manufacturing, Northwestern Polytechnical University, Xi'an, China

Abstract

This conference short paper presents a numerical design route for programmable hyperbolic metamaterials formed by mixing chiral and achiral unit cells within a unified parametric family. A regular $5 \times 4 \times 3$ lattice assembly is parameterized and converted into beam-based finite-element models for quasi-static compression, first-order modal analysis, and PSD-based random-vibration evaluation. Based on 21 randomly generated hybrid layouts with prescribed achiral fractions, the accessible performance space is quantified in terms of equivalent stiffness, first-order natural frequency, and acceleration root-mean-square (RMS). The results show that increasing the achiral fraction raises stiffness and modal frequency but aggravates the random-vibration response, revealing a pronounced stiffness–isolation trade-off. A binary genetic-algorithm framework is then used to optimize the unit-cell distribution for stiffness maximization, first-mode maximization, RMS minimization, and RMS minimization under a stiffness constraint. The optimized layouts indicate that stiffness- and frequency-driven objectives favor vertically continuous achiral load paths, whereas vibration-oriented objectives disrupt

those paths and, under stiffness constraints, evolve toward layered compromise patterns. The study therefore provides a concise and reusable numerical route for programmable performance allocation in lattice support structures.

Keywords: programmable metamaterials, hybrid lattice, stiffness–vibration trade-off, hyperbolic unit cell, genetic algorithm, fast design

1 Introduction

Mounting and support structures in aerospace systems are frequently required to satisfy two conflicting requirements: high static stiffness for load transfer and low dynamic transmissibility for vibration protection [1–5]. Conventional solutions usually strengthen the structure by adding material or stiffeners, but this often shifts the structure toward poorer isolation performance in broadband vibration environments. Mechanical metamaterials offer a more flexible route because their effective behavior is governed by geometry rather than chemistry alone [6–9]. Recent studies on programmable metamaterials have shown that unit-cell design can be used to tune stiffness, damping, and low-frequency isolation performance in a controllable manner [10–12].

A limitation of single-topology graded lattices is that they inherit one dominant load-transfer mechanism, so the accessible performance envelope remains bounded even when geometric parameters are graded [13]. Hybrid lattices can enlarge that envelope by combining multiple unit-cell topologies in one structure [14–16]. However, practical use is often hindered by geometric incompatibility between different cells and by the need for complex transition regions [17]. To overcome this difficulty, our previous work introduced a hyperbolic metamaterial family in which chiral and achiral cells are generated from the same parameterized template [18, 19]. This common geometric language makes it possible to mix the two cell types without additional interface design.

The present short paper condenses the numerical part of the full manuscript and follows the route required for conference submission: geometric parameterization, programmable performance-space verification, stiffness optimization, first-order modal-frequency optimization, vibration-suppression optimization, and vibration-suppression optimization under a stiffness constraint. Experimental validation is intentionally omitted here and reserved for the full-length paper.

2 Unified Parametric Model of the Hybrid Hyperbolic Lattice

2.1 Geometric parameterization

The hybrid lattice is assembled from two unit-cell variants belonging to the same hyperbolic family, as shown in Fig. 1. Each cell consists of upper and lower polygonal frames connected by inclined struts. The geometry is controlled by the polygon side length a, cell height h, frame radius R_{f}, inclined-strut radius R_{l}, polygon-edge number n, and a step-connection parameter inc. By varying inc, the unit cell switches

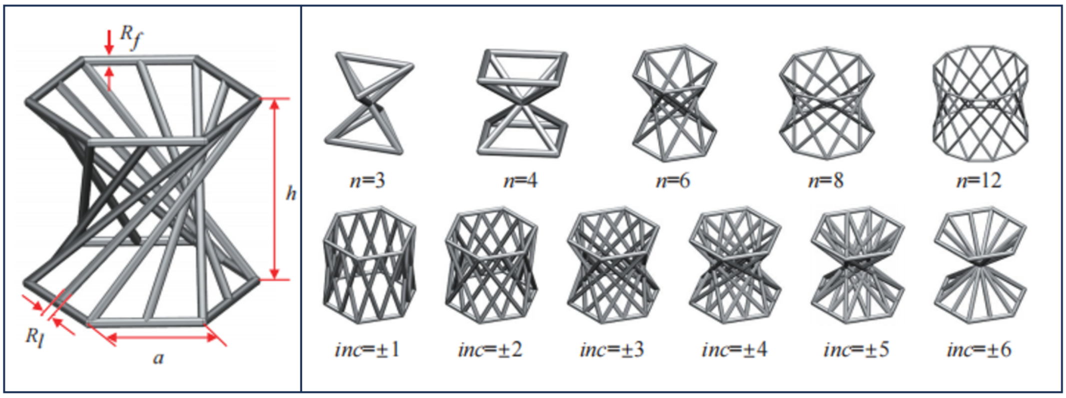

Figure 1: Unified parameterization of the hyperbolic unit-cell family. The chiral and achiral variants are generated within the same geometric framework and can therefore be mixed directly in one lattice assembly.

continuously between an achiral load-bearing topology and a chiral topology with tension–torsion coupling. An additional middle hexagonal ring is introduced in the chiral version to avoid self-locking during tessellation while preserving geometric compatibility with the achiral cell [18].

In the present study, a regular $5 \times 4 \times 3$ assembly is used, giving $N_c = 60$ cell positions. Each position is encoded by a binary design variable,

$$x_i \in \{0, 1\}, \qquad i = 1, 2, \ldots, N_c, \tag{1}$$

where $x_i = 0$ denotes a chiral cell and $x_i = 1$ denotes an achiral cell. Because both variants share the same outer dimensions and tessellation rules, all candidate structures preserve the same global envelope and relative density while changing only the internal distribution of load paths.

2.2 Finite-element evaluation models

All numerical evaluations are performed with three-dimensional beam models because the hyperbolic lattice is composed of slender struts. The base material is stainless steel with $E = 206\,\mathrm{GPa}$, $\nu = 0.3$, and a constant strut diameter of 0.5 mm. The bottom surface is coupled to a reference point and fully clamped in all six degrees of freedom. For quasi-static compression, the top surface is coupled to a second reference point whose in-plane translations and rotations are fixed, while the out-of-plane displacement is prescribed. For modal and random-vibration analyses, the same support pattern is retained and a 5 kg tip mass is attached at the top reference point.

Three simulation models are used throughout this work: (i) quasi-static compression to extract equivalent axial stiffness, (ii) eigenvalue analysis to obtain the first natural frequency, and (iii) PSD-based random-vibration analysis to evaluate the acceleration RMS at the top reference point. The random-vibration excitation follows the established base-acceleration spectrum with breakpoints at 20, 80, 350, and 2,000 Hz, including

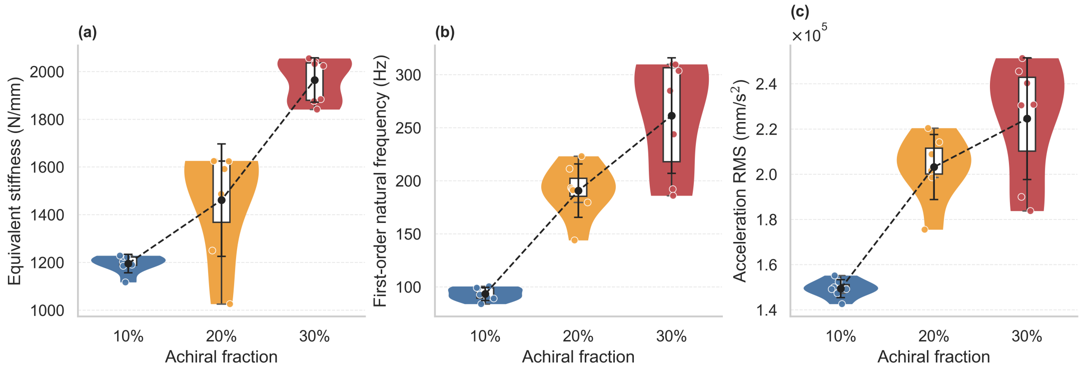

Figure 2: Programmable performance space of the $5 \times 4 \times 3$ hybrid lattice obtained from 21 random configurations. Violin plots show the distribution within each achiral-fraction group, white boxes indicate quartiles, and dashed black lines connect the group means with one-standard-deviation error bars. Increasing the achiral fraction improves stiffness and first-order frequency but also increases vibration response, revealing a clear stiffness–isolation trade-off.

the plateau in the 80 Hz to 350 Hz band used in the full manuscript.

3 Programmable Performance Space Verification

To quantify how spatial distribution alone affects the structural response, 21 hybrid configurations are generated automatically: seven random layouts for each prescribed achiral fraction of 10%, 20%, and 30%. The resulting statistics are summarized in Fig. 2 and Table 1.

Two observations are immediate. First, the three metrics are all highly tunable even though the outer dimensions and total cell number are fixed. The mean equivalent stiffness increases from 1,195.1 N/mm at 10% achiral fraction to 1,964.2 N/mm at 30%, which corresponds to a 64.4 % increase. The first-order natural frequency rises even more strongly, from 93.4 Hz to 261.3 Hz, i.e., a 179.8 % increase. Second, this improvement in load-bearing and dynamic stiffness is accompanied by a systematic growth in vibration response: the mean acceleration RMS increases from 1.49×10^5 to 2.25×10^5 mm/s^2, an increase of 50.3 %.

The dispersion within each group confirms that the structure is not controlled by cell ratio alone. At the same achiral fraction, different spatial arrangements still produce notable changes in all three metrics. This spread is especially clear for the 20 % stiffness group and for the 30 % modal and RMS groups, showing that the through-thickness connectivity and lateral clustering of achiral cells remain important design variables even under a fixed cardinality constraint. Therefore, the mixed hyperbolic lattice provides not merely a graded material fraction, but a broad programmable performance space in which stiffness, resonance, and vibration transmission can be redistributed by topology.

Table 1: Statistical summary of the programmable performance space for the 21 sampled configurations.

Metric	10%	20%	30%
Equivalent stiffness (N/mm)	1195.1 ± 38.5	1460.8 ± 235.4	1964.2 ± 92.8
First modal frequency (Hz)	93.4 ± 6.2	190.6 ± 25.2	261.3 ± 54.4
Acceleration RMS (mm/s^2)	$1.49 \times 10^5 \pm 0.04 \times 10^5$	$2.03 \times 10^5 \pm 0.14 \times 10^5$	$2.25 \times 10^5 \pm 0.27 \times 10^5$

4 Optimization Framework and Numerical Results

4.1 Binary GA formulation

The unit-cell distribution is optimized with a binary genetic algorithm (GA). The general optimization problem is written as

$$\begin{aligned} &\min_{\boldsymbol{x}} F(\boldsymbol{x}) \\ &\text{s.t. } x_i \in \{0,1\}, \qquad i = 1, \ldots, N_c, \\ &\sum_{i=1}^{N_c} x_i = K, \quad K = \text{round}(v_f N_c), \end{aligned} \tag{2}$$

where v_f is the prescribed achiral fraction when a fixed-ratio study is performed. Depending on the design target, $F(\boldsymbol{x})$ is replaced by the negative equivalent stiffness, the negative first-order natural frequency, the acceleration RMS, or the acceleration RMS together with an additional stiffness constraint. The implemented MATLAB solvers provided in the workspace were used directly. In the present conference version, the stiffness, first-mode, and RMS single-objective cases are all reported under the same fixed achiral fraction of $v_f = 20\%$, whereas the constrained vibration-suppression case allows the ratio to evolve freely while satisfying the prescribed stiffness band.

4.2 Stiffness optimization

For displacement-controlled compression, the equivalent stiffness is defined as

$$k_{\text{eff}}(\boldsymbol{x}) = \frac{|R_z(\boldsymbol{x})|}{|u_0|}, \tag{3}$$

where R_z is the resultant top reaction force and u_0 is the prescribed vertical displacement. Maximizing k_{eff} yields the layout shown in Fig. 3(a). The achiral cells preferentially stack along the loading direction and form vertically connected column-like load paths. This pattern is mechanically intuitive: the achiral cell is more favorable for axial force transfer, so continuous achiral chains strengthen the through-thickness stiffness and reduce load redistribution through the more compliant chiral network. The regenerated optimum from the workspace solver reaches $k_{\text{eff}} = 1.74 \times 10^4$ N/mm.

4.3 First-order modal-frequency optimization

The first natural frequency is optimized by solving

$$\max_{\boldsymbol{x}} \; f_1(\boldsymbol{x}), \tag{4}$$

subject to the same binary encoding and cardinality constraint. After resetting the cardinality constraint to the common 20% achiral fraction, the regenerated solver optimum reaches 271.2 Hz. As shown in Fig. 3(b), the corresponding topology becomes visually identical to the stiffness-optimized layout in the present study, indicating that the dominant first mode is governed by the same vertically efficient achiral load path that controls quasi-static stiffness. This consistency further supports the interpretation that strengthening the through-thickness dynamic load-transfer chain is also the most effective way to push the first resonance upward under the current boundary condition and tip-mass setting.

4.4 Vibration-suppression optimization

For random vibration, the design target is the acceleration RMS at the top reference point,

$$a_{\mathrm{RMS}}(\boldsymbol{x}) = \left(\int_{f_{\min}}^{f_{\max}} S_a(f;\boldsymbol{x})\,\mathrm{d}f \right)^{1/2}, \tag{5}$$

where S_a is the response PSD. Minimizing a_{RMS} under the fixed 20 % achiral fraction leads to the layout in Fig. 3(c). In contrast to stiffness maximization, the optimizer suppresses long, vertically continuous achiral columns. The resulting topology keeps most of the lattice chiral and confines the achiral cells to a more localized region, which weakens direct transmission paths from the base to the top mass. The regenerated optimum gives $a_{\mathrm{RMS}} = 5.86 \times 10^4$ mm/s^2.

4.5 Vibration suppression with stiffness constraint

A more practical formulation is to minimize vibration while preserving a minimum load-bearing capability:

$$\begin{aligned} &\min_{\boldsymbol{x}} \; a_{\mathrm{RMS}}(\boldsymbol{x}) \\ &\text{s.t. } 1.7 \times 10^4 \le k_{\mathrm{eff}}(\boldsymbol{x}) \le 2.5 \times 10^4 \text{ N/mm}, \\ &\quad\; x_i \in \{0,1\}. \end{aligned} \tag{6}$$

The optimum in Fig. 3(d) no longer resembles either of the single-objective extremes. Instead, it develops a layered compromise: an upper achiral-rich framework preserves stiffness, while the lower region remains more chiral-dominated and compliant to mitigate vibration transmission. The regenerated solution satisfies $k_{\mathrm{eff}} = 1.72 \times 10^4$ N/mm and reduces the reported RMS to 4.26×10^3 mm/s^2. This result highlights the main advantage of the programmable hybrid lattice: once the chiral and achiral cells are geometrically compatible, the optimizer can reallocate them to meet different design goals without changing the external envelope.

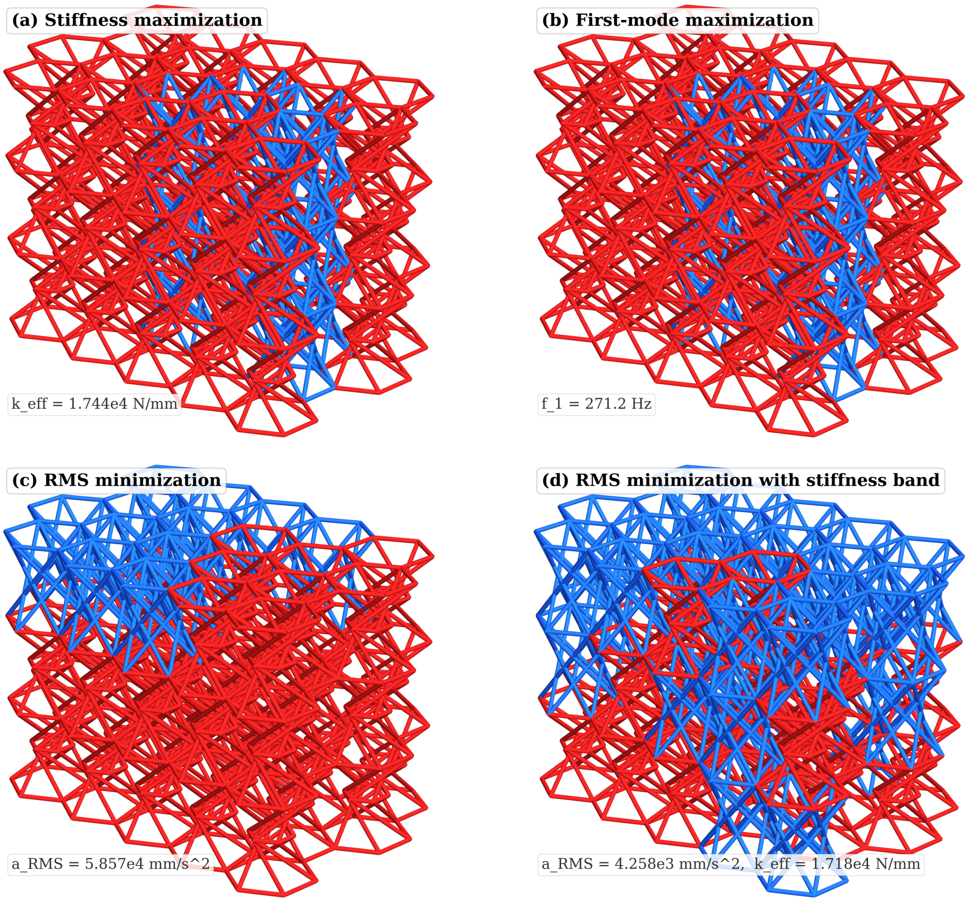

Figure 3: Representative optimization results obtained with the MATLAB solvers in the workspace. Achiral cells are shown in blue and chiral cells in red. (a) Stiffness maximization promotes vertically continuous achiral columns. (b) Under the present 20% achiral-ratio constraint, first-mode maximization converges to the same topology as stiffness maximization. (c) RMS minimization suppresses through-thickness stiff chains and retains a chiral-dominated body. (d) RMS minimization with a stiffness band produces a layered compromise between load-bearing and vibration isolation.

5 Conclusions

This conference paper established a compact numerical workflow for designing programmable hyperbolic metamaterials by redistributing geometrically compatible chiral and achiral cells within a fixed lattice envelope. The unified parametric model enables direct mixing of the two unit-cell families without transition regions, while the 21-layout verification study confirms that the hybrid lattice offers a broad programmable space in equivalent stiffness, first-order frequency, and random-vibration response. Increasing the achiral fraction systematically strengthens the structure and raises the first modal frequency, but it also increases broadband vibration transmission, thereby making the stiffness–isolation trade-off explicit at the structural level.

The four optimization studies further clarify the governing topology–performance relation. Under the common 20% achiral-ratio constraint, stiffness and first-mode optimization both favor vertically connected achiral load paths, whereas RMS minimization suppresses continuous through-thickness stiff chains. When vibration reduction is pursued under a stiffness band, the optimal structure no longer follows either single-objective extreme, but instead develops a layered compromise that preserves load-bearing capability while limiting vibration transmission. Taken together, these results define the numerical core of the full study and show that programmable allocation of cell topology can serve as an effective design lever for simultaneously managing stiffness and vibration requirements in lattice support structures. Experimental validation and manufacturing considerations will be reported in the full-length paper.

References

[1] W. Hu, Z. Zhou, S. Zhou, R. Hao, T. Chen, T. Sun, Vibration suppression of two-panel structure via stiffness-tunable joints, International Journal of Mechanical Sciences 300 (2025) 110487. doi:10.1016/j.ijmecsci.2025.110487.

[2] Q. Liu, J. Yu, Z. Wang, H. Cheng, S. Chen, L. Zhang, Optimization design for support points of the body-mounted solar panel, Aerospace 12 (1) (2025). doi:10.3390/aerospace12010006.

[3] S. M. R, N. Ac, B. Dattaguru, Aero structural and electromagnetic design optimisation of maritime patrol aircraft radome using direct search algorithms, Defence Science Journal 73 (2023) 394–401. doi:10.14429/dsj.73.17889.

[4] R. Reda, Y. Ahmed, I. Magdy, H. Nabil, M. Khamis, M. A. Lila, A. Refaey, N. Eldabaa, M. A. Elmagd, A. E. Ragab, A. Elsayed, Wall panel structure design optimization of a hexagonal satellite, Heliyon 10 (2) (2024) e24159. doi:10.1016/j.heliyon.2024.e24159.

[5] Y. Haddad, J. Feng, On the trade-off between damping and stiffness in the design of discontinuous fibre-reinforced composites, Composites Part B: Engineering 34 (1) (2003) 11–20. doi:10.1016/S1359-8368(02)00076-8.

[6] Fayyaz, S. Bashmal, A. Nazir, S. Khan, A. Alofi, Damping optimization and energy absorption of mechanical metamaterials for enhanced vibration control applications: A critical review, Polymers 17 (2) (2025). doi:10.3390/polym17020237.

[7] Fayyaz, S. Bashmal, A. Nazir, S. Khan, A. Alofi, Damping optimization and energy absorption of mechanical metamaterials for enhanced vibration control applications: a critical review, Polymers 17 (2) (2025) 237.

[8] M. Shojaee, I. Valizadeh, D. K. Klein, P. Sharifi, O. Weeger, Multiscale modeling of functionally graded shell lattice metamaterials for additive manufacturing, Engineering with Computers 40 (3) (2024) 2019–2036.

[9] C. Liu, X. Zhang, J. Chang, Y. Lyu, J. Zhao, S. Qiu, Programmable mechanical metamaterials: basic concepts, types, construction strategies—a review, Frontiers in Materials 11 (2024) 1361408.

[10] X. Fang, J. Wen, L. Cheng, Programmable gear-based mechanical metamaterials, Nature Materials 21 (2022) 869–876.

[11] Q. Zhang, D. Guo, G. Hu, Tailored mechanical metamaterials with programmable quasi-zero-stiffness features for full-band vibration isolation, Advanced Functional Materials 31 (33) (2021).

[12] H. Huang, R. Pi, Z. Li, X. Yu, Compression and vibration isolation properties of metamaterials with variable Poisson's ratios and cosine-shaped beams, Materials & Design 262 (2026) 115445. doi:10.1016/j.matdes.2026.115445.

[13] D. L. Ramirez-Gutierrez, E. Cuan-Urquizo, A. Roman-Flores, Functionally graded sinusoid-based metamaterials: Towards tailoring effective mechanical properties and deformation modes with a single design parametric function, Materials & Design 262 (2026) 115423. doi:10.1016/j.matdes.2025.115423.

[14] S. Rahimi, M. Asghari, Design and evaluation of two proposed hybrid FCC-BCC lattice structures for enhanced mechanical performance, Heliyon 11 (1) (2025) e40911. doi:10.1016/j.heliyon.2024.e40911.

[15] X. Yang, Y. Gong, L. Zhao, J. Zhang, N. Hu, Compressive mechanical properties of layer hybrid lattice structures fabricated by laser powder bed fusion technique, Journal of Materials Research and Technology 22 (2023) 1800–1811.

[16] D. Syrlybayev, A. Perveen, D. Talamona, Experimental investigation of mechanical properties and energy absorption capabilities of hybrid lattice structures manufactured using fused filament fabrication, The International Journal of Advanced Manufacturing Technology 125 (5) (2023) 2833–2850.

[17] Y. Liu, Y. Wang, H. Ren, et al., Ultrastiff metamaterials generated through a multilayer strategy and topology optimization, Nature Communications 15 (2024) 2984.

[18] L. Meng, J. Shi, C. Yang, T. Gao, Y. Hou, L. Song, D. Gu, J. Zhu, P. Breitkopf, W. Zhang, An emerging class of hyperbolic lattice exhibiting tunable elastic properties and impact absorption through chiral twisting, Extreme Mechanics Letters 40 (2020) 100869.

[19] L. Meng, M. Zhong, Y. Gao, T. Gao, Y. Hou, J. Zhu, P. Breitkopf, W. Zhang, Impact resisting mechanism of tension–torsion coupling metamaterials, International Journal of Mechanical Sciences 272 (2024) 109100.